Segmentation of deep grey matter structures by using magnetic resonance high-resolution T1-weighted images acquired at 3 Tesla: a technical approach

Fernanda Sofia Quintela da Silva Brandão

2010

Mestrado em Informática Médica

Faculdade de Ciências | Faculdade de Medicina

Universidade do Porto

Orientador: António José de Bastos Leite, Professor Auxiliar de Radiologia e Imagem Médica, Serviço de Imagiologia Médica da Faculdade de Medicina da Universidade do Porto

Co-orientador: José Maria Amaral Fernandes, Professor Auxiliar do Departamento de Electrónica, Telecomunicações e Informática da Universidade de Aveiro.

Table of contents

Agradecimentos

Agradeço ao meu orientador, Prof. Doutor António José de Bastos Leite, pela ideia do trabalho e pelo apoio no decurso do seu desenvolvimento.

Agradeço ao Prof. Doutor José Maria Fernandes, co-orientador, pela ajuda na estruturação do trabalho, pelas dicas e pelo apoio.

Agradeço ao Prof. Doutor Miguel Coimbra, ao Prof. Doutor Ricardo Correia e ao Prof. Doutor Luís Antunes, pelo apoio adicional.

Agradeço à Prof. Doutora Isabel Ramos, por acreditar em mim.

Agradeço a todos os participantes da amostra, sem os quais o trabalho não teria sido possível.

Agradeço ao Rui, por ser há anos o meu melhor amigo e marido paciente.

Agradeço aos meus pais, pela preocupação.

Agradeço aos meus amigos, por me mimarem.

Agradeço aos outros, porque também me fazem mexer.

Agradeço a mim, por ter finalizado esta etapa.

Preamble

The establishment of regular research sessions using brain magnetic resonance imaging (MRI) with a scanner operating at 3 Tesla (T) led us into the issue of choosing appropriate MRI sequences, given the technical challenges raised by ultra high field (≥3 T) MRI.

Scientific publication

The original work developed for this thesis was published in the form of a scientific article: Magnetisation-prepared rapid gradient-echo versus inversion recovery turbo spin-echo T1-weighted images for segmentation of deep grey matter structures at 3 T. Clinical Radiology 2016;71(12): 1304–1308.

Sumário

O objectivo do estudo que conduziu a esta tese foi comparar as sequências de ressonância magnética (RM) 3D *magnetisation-prepared rapid gradient-echo* (MPRAGE) e *inversion recovery turbo spin-echo* (IR TSE) como fonte de imagens ponderadas em T1 para segmentar o estriado e o tálamo. Imagens 3D MPRAGE e IR TSE ponderadas em T1 foram adquiridas a 30 adultos jovens num equipamento de RM 3 Tesla. Foi aplicado às imagens um algoritmo de segmentação automática combinando intensidade de sinal/contraste e informação anatómica. Os resultados mostraram que a sequência IR TSE é melhor que a sequência 3D MPRAGE como fonte de imagens ponderadas em T1 para segmentar a parte posterior do estriado e a parte lateral do tálamo.

Abstract

The aim of the study leading to this thesis was to compare three-dimensional (3D) magnetisation-prepared rapid gradient echo (MPRAGE) with inversion recovery (IR) turbo spin-echo (TSE) T1-weighted magnetic resonance imaging sequences as a source of input images to segment the striatum and thalamus. 3D MPRAGE and IR TSE T1-weighted images (T1-WI) were acquired from 30 young adult subjects using a scanner operating at 3 Tesla. An automatic segmentation algorithm combining signal intensity/contrast and anatomic information was applied to the images. The results have shown that IR TSE serves as a better source of T1-WI than 3D MPRAGE to segment the posterior part of the striatum and the lateral part of the thalamus.

Outline of the thesis

Chapter 1 covers theoretical concepts of magnetic resonance (MR) focusing on issues like high field strength, T1 relaxation times, and standing wave effects. Some T1-weighted MR imaging (MRI) sequences are also described.

Chapter 2 specifically focuses on segmentation of deep grey matter structures. The most frequently used segmentation strategies are briefly mentioned.

After a section presenting suggestions for further reading, the scientific article corresponding to the original work developed for this thesis is included as an attachment.

1. Magnetic resonance imaging at high field strength: an overview

1.1. Magnetic resonance imaging as a morphological insight into the brain

Magnetic resonance imaging (MRI) has become a leading neuroimaging technique. It represents the state of the art for morphological visualization of the human brain.

Unlike computed tomography, in which tissue contrast is determined by differences in electronic density, the relative contrast between brain structures is not constant on MRI. Magnetic resonance (MR) images are generated by measuring the behaviour of hydrogen protons exposed to a magnetic field. When a radiofrequency (RF) pulse is applied at the same frequency of their Larmor precession, a phenomenon known as MR occurs and hydrogen protons enter a high-energy state. After this phenomenon, proton relaxation begins and the energy is re-emitted. A coil captures and measures this energy, which is proportional to the quantity of hydrogen protons. Proton density (PD) and the proportion of free and bound protons influence the relaxation times, and hence different tissues have different intensities on the final MR image.

MRI pulse sequences used in clinical practice generally correspond to spin-echo (SE), turbo spin-echo (TSE), or gradient-echo (GRE) sequences. TSE sequences are also commonly called fast spin echo.

Choosing specific times to emit RF pulses and to register their echoes highlights differences between tissues or lesions. Different values for the echo time (TE) and the RF pulse repetition time (TR) provide different and specific image contrasts. T1-weighted images (T1-WI) usually offer higher contrast between grey matter (GM) and white matter (WM) than PD-weighted images or T2-weighted images (T2-WI). T2-WI provide high contrast between cerebrospinal fluid (CSF) and the brain tissue. On fluid-attenuated inversion recovery (FLAIR) images, the signal intensity of CSF is suppressed.

A paramagnetic contrast agent can also be used to identify and characterise lesions. The interpretation of MRI requires the combined information of multiple pulse sequences and different image weightings.

1.2. Brain magnetic resonance imaging at high field strength

1.2.1. Technical considerations

3 Tesla (T) MRI has been generally introduced in clinical practice during the past decade. It offers substantially higher signal-to-noise and contrast-to-noise ratios than 1.5 T MRI. 3 T MRI can be used to improve spatial resolution or to shorten image acquisition times.

The advent of high field MRI led to the issue of pulse sequence optimisation, given that some imaging sequences and many parameters at 1.5 T are not well suited for 3 T MRI. This can be explained by differences in hydrogen behaviour as the magnetic field strength increases.

At high field strength, the Larmor frequency increases. Therefore, the RF specific absorption rate (SAR) increases as well. Limits for SAR may require a compromise in the RF pulse sequence timing and in the corresponding flip angles. Such compromise may result in altered image contrast or in prolongation of the acquisition times.

At high field strength, there are larger chemical shift imaging and susceptibility-induced artefacts that can lead to signal loss.

Chemical shift imaging and susceptibility artefacts at high field strength can be partly counteracted by performing parallel imaging, increasing the RF pulse bandwidth, or shortening the TE.

RF pulse field inhomogeneity is also a major concern when acquiring images at high field strength, because it often leads to the so-called standing wave (or "dielectric") effects, and to subsequent large local variations in signal intensity.

1.2.2. T1 relaxation times and tissue contrast

The primary sources of tissue contrast on MRI are the following: longitudinal relaxation (T1), transverse relaxation (T2), and the intrinsic PD. To better understand the influence of T1 relaxation on image contrast at high field strength, the following additional explanation on MR is given.

When exposed to an external magnetic field, the hydrogen protons of the body align with the field (Figure 1a). As previously mentioned, the hydrogen protons absorb energy (resonate) and generate the MR signal when the subject is exposed to a RF pulse matching the frequency of their Larmor precession. The larger the generated magnetisation is, the stronger the signal induced in the receiver coil will be.

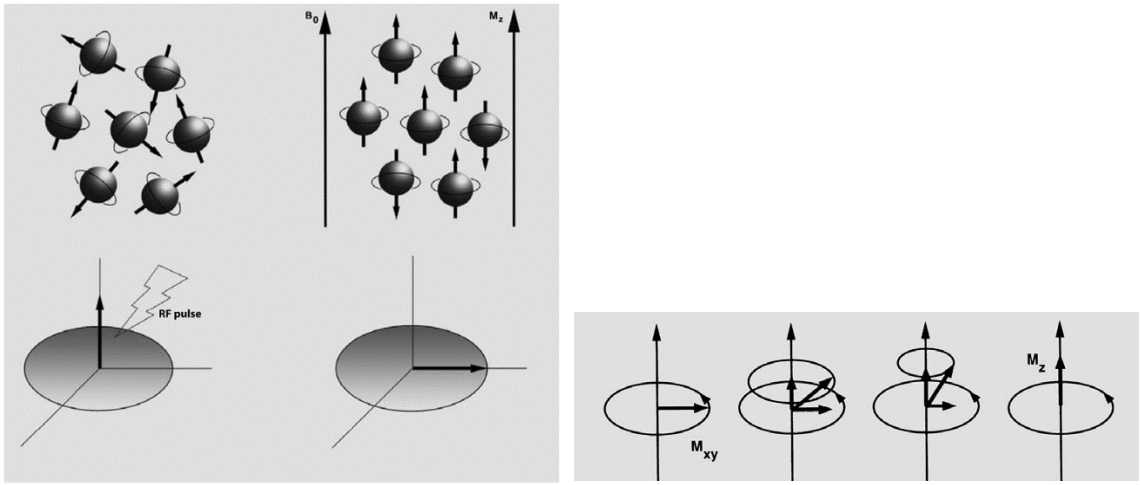

a) b)

Figure 1. Proton excitation and relaxation processes. Spin orientation is changed by the radiofrequency pulse, which tilts the net magnetisation vector into the transverse (Mxy) plane (a), inducing the signal to be received in the coil. Some time after this, T2 and T1 relaxation processes take place, and the net magnetisation vector re-aligns with the magnetic field (b). Adapted from Weishaupt, Köchli et al. 2006.

Upon formation of the MR signal, decoherence of transverse nuclear spin magnetisation takes place, and leads to the so-called spin-spin or T2 relaxation phenomenon. Later, the longitudinal magnetisation tends to realign, and the spin-lattice or T1 relaxation phenomenon occurs, as displayed on Figure 1b.

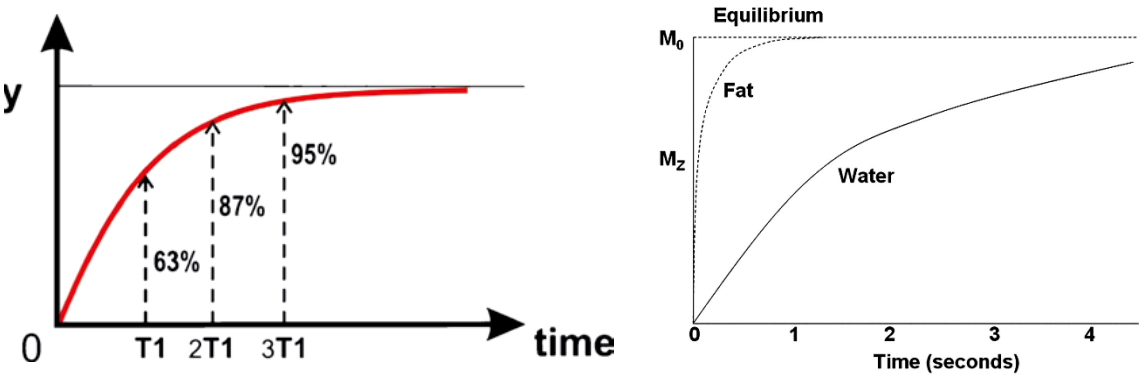

a) b)

Figure 2. T1 relaxation of fat and water. The relaxation phenomenon can be displayed as a time to signal intensity curve (a). Depending on the tissue composition, the net magnetisation vector recovery can be shorter or longer, and hence signal intensity at a given time is different (b).

A T1 relaxation curve is shown on Figure 2a. The T1 relaxation time corresponds to the time that the net magnetisation vector recovers 63%. As can be seen on Figure 2b, the relaxation process (c.f., time) depends on the tissue type. T1 relaxation times of free water are up to 4 seconds. By contrast, in tissues like fat, where the protons are partly bound or motion-restricted, T1 relaxation times are short—around 400 to 800 ms. T1 relaxation times were found to be relatively high in the cortical GM (around 1100 ms), intermediate in the basal ganglia, and relatively low in the thalamus (between 750 and 850 ms) at 1.5 T. Structures like the splenium of the corpus callosum and the frontal WM were found to

present shorter T1 relaxation times (around 600 ms) than the caudate nucleus or the putamen (> 900 ms) at 1.5 T.

The longer the T1 relaxation time, the lower the signal intensity on T1-WI. Hence, GM is hypointense relative to the WM on T1-WI, given that WM generally has shorter T1 relaxation times than GM. For the same reason, the thalamus presents higher signal intensity on T1-WI than the basal ganglia, because of its higher myelin content.

At high field strength, the T1 relaxation process takes much longer. Crucially, the increase in T1 relaxation times of the GM at high field strength is at least 70% more than the increase in T1 relaxation times of the WM.

Figures 3a to 3c show how the increase in field strength influences T1 magnetisation recovery of the WM (solid curve) and the GM (top dashed curve) on a FLAIR sequence. As can be seen on the diagrams, the T1 magnetisation recovery curves for WM and GM at 3 T (Figure 3b) and 7 T (Figure 3c) indicate slightly lower longitudinal magnetisation than at 1.5 T (Figure 3a).

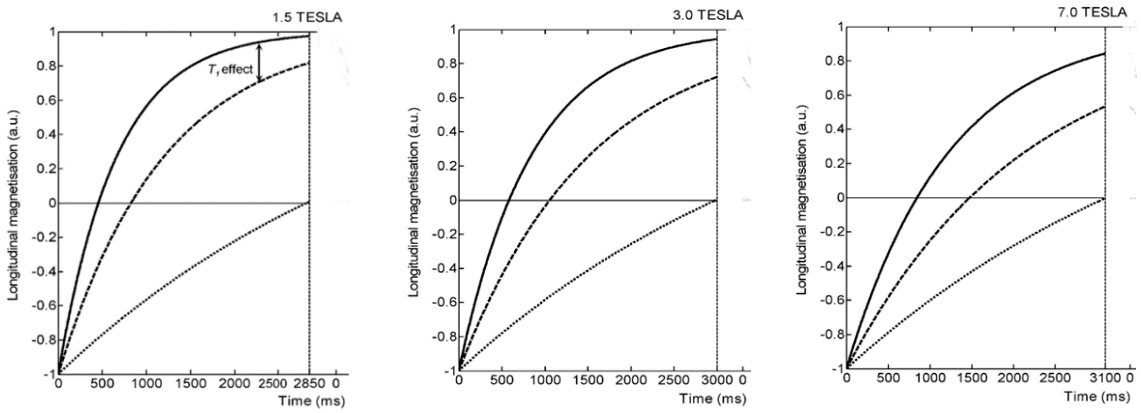

Figure 3. T1 recovery on a fluid-attenuated inversion recovery sequence at 1.5, 3, and 7 Tesla. Adapted from European Radiology 2010;20(4): 915–922.

1.2.3. Standing wave effects

The RF pulse field may become inhomogeneous due to shortening of RF wavelengths caused by conductive and dielectric effects in the tissue, which are exacerbated at high field strength and typically appear as an artefactual brightness in the centre of images (Figure 4).

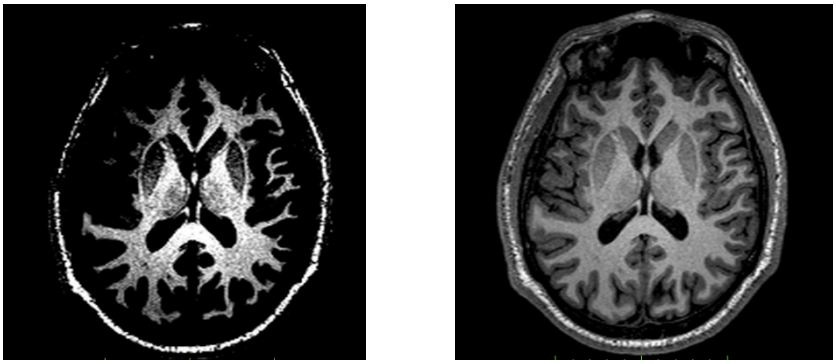

a) b)

Figure 4. Standing wave effects at 3 Tesla affect the signal intensity of images. If a "narrow" window is selected (a), a central area of higher signal intensity can be seen on the image. This feature must not affect diagnostic accuracy, and usual windowing (b) typically reveals a more homogeneous appearance.

Surface coils and the use of pads filled with a medium with high electric conductivity and permittivity can significantly homogenise the RF distribution in tissues. This has been applied to optimise MR sequences for abdominal examinations. For neuroimaging applications, the production of phased-array small-element head coils allowed reconstruction of brain images with higher uniformity.

The effect of RF inhomogeneity on MR not only affects the global appearance of the images, but may also introduce difficulties in segmentation procedures. This issue encouraged the development of signal intensity inhomogeneity (bias) correction.

1.3. T1-weighted magnetic resonance imaging sequences

Two-dimensional (2D) SE or TSE sequences do not allow acquisition of images with optimal GM to WM contrast at 3 T. 2D SE or TSE sequences are prone to high field shielding effects induced by eddy currents, which prevent central parts of the tissue to be properly excited. In addition, magnetisation transfer (MT) effects are enhanced at high field strength in this type of sequences. Both of the issues contribute to lack of contrast.

The three-dimensional (3D) magnetisation-prepared rapid GRE (MPRAGE) sequence is well suited for high field imaging. It is a magnetisation-prepared sequence, because it uses a 180º preparation (pre)pulse before the RF excitation pulse, which has a very small flip angle, and then low SAR. Significant parameters of the 3D MPRAGE sequence include the time between the preparation pulse and the start of readout (inversion time [TI]), and the

recovery time after the readout until the next repetition. The TI is particularly important to obtain excellent GM to WM contrast. It has to be short enough to minimise its effect on the recovery curve, but large enough to provide longitudinal magnetisation and the best possible signal intensity. A TI value of 900 ms was found to be the most appropriate at 3 T. To reduce inhomogeneities of the RF pulses and the related effects on the receiver coil, the duration of the RF excitation pulse needs to be short. A duration of nearly 1.3 ms is compatible with the short TE and the relatively short TR used to acquire 3D MPRAGE T1-WI with very high resolution (voxels with approximately 1 mm^3) within an acceptable acquisition time (up to 13 minutes).

Inversion recovery (IR) sequences can also generate high-resolution T1-WI. The original IR SE sequences had several limitations (e.g., long acquisition times), which have been reduced using TSE sequences (i.e., filling several lines of the k-space during each TR). IR sequences rely on the application of an inversion RF pulse (i.e., a RF pulse that flips 180º the longitudinal magnetisation), before the RF excitation pulse. The choice of an inversion time of 400–800 ms provides optimal GM to WM contrast on IR T1-WI. Our experience led to the choice of 400 ms as the preferred TI at 3 T to obtain optimal IR TSE T1-WI.

As previously mentioned, the longitudinal magnetisation recovery occurs as a function of the tissue T1 relaxation times. At the time of readout, tissue magnetisation can be positive or negative, depending on the selected TI and the tissue itself. Therefore, with an appropriate reconstruction algorithm, IR images have the potential to provide a wider range of contrast than other types of T1-WI, because the positive and negative signal intensity values are taken into account.

2. Segmentation of deep grey matter structures

Segmentation consists in partitioning, according to an underlying morphological classification. One of the most frequently addressed brain segmentation strategies is the partitioning into grey matter (GM), white matter (WM) and cerebrospinal fluid. As previously mentioned, T1-weighted images (T1-WI) are those that best display the anatomy of the brain, and provide the highest contrast between GM and WM. For this reason, most brain segmentation analyses use T1-WI.

The delineation and volume estimation of deep GM structures remains a challenging task, due to the small size and anatomical variability of these structures, the occurrence of partial volume effects, or even the lack of contrast between GM and WM. These issues require appropriate frameworks to enhance segmentation results. Figure 5 shows differences in contrast and signal intensity of deep GM structures among different types of T1-weighted magnetic resonance (MR) imaging sequences acquired at 3 Tesla. Given that T1 relaxation times are strongly dependent on the magnetic field strength, their prolongation at high field strength results in reduced contrast, especially on standard T1-weighted spin-echo sequences.

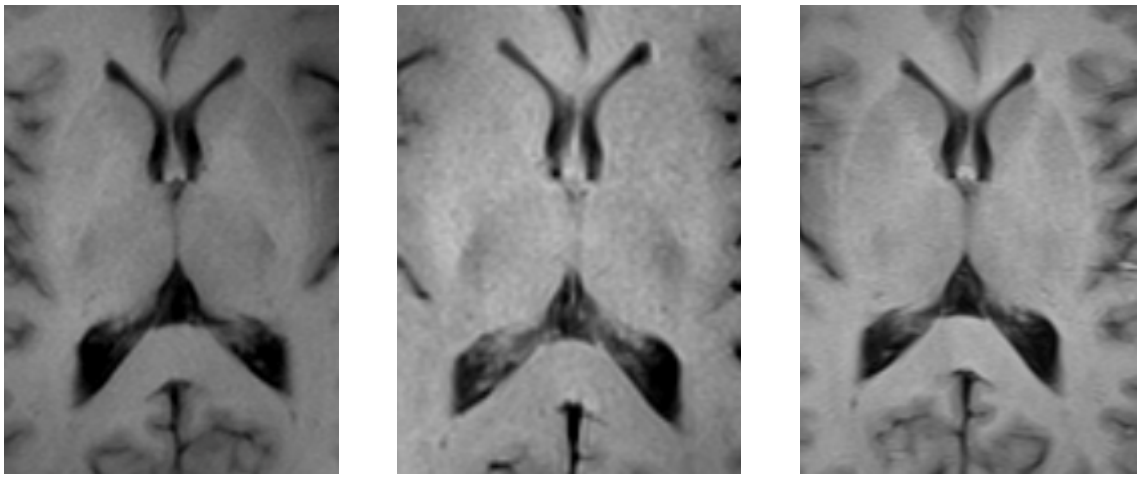

a) b) c)

Figure 5. T1-weighted magnetic resonance images acquired at 3 Tesla. Gradient-echo (a) and fluid-attenuated inversion recovery (c) images display higher contrast between deep grey matter nuclei and the surrounding white matter than the spin-echo (b) image.

2.1. Deep grey matter structures

Deep GM corresponds to a group of interconnected subcortical nuclei that represent one of the fundamental processing units of the brain. They include the striatum (i.e., the caudate nucleus and the putamen) and diencephalic nuclei with a different embryological origin, such as the thalamus (Figure 6).

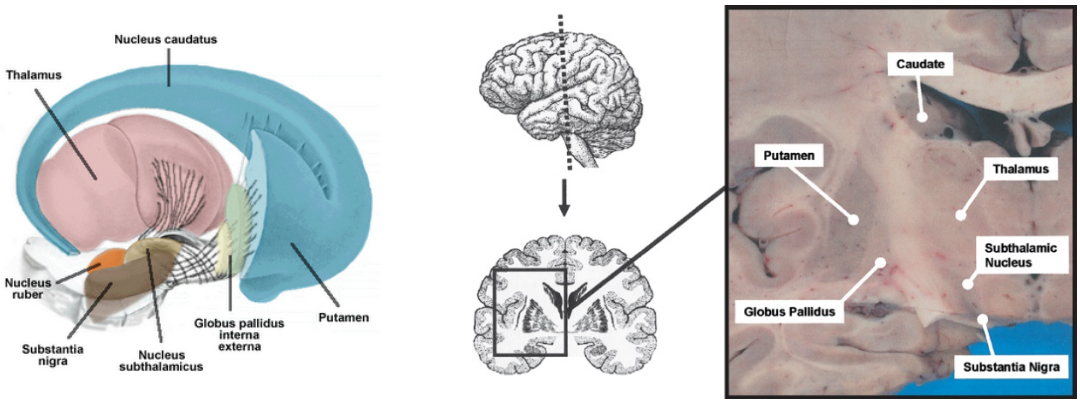

Figure 6. The human deep grey matter nuclei. The deep grey matter is composed by a group of nuclei close in position and functionally related (source: www.profelis.org/).

2.2. Segmentation

Accurate segmentation of subcortical structures, such as the striatum and thalamus, on MR images is challenging, because the specific anatomical and tissue properties of these structures often result in limited contrast.

The most common segmentation approaches are based on tissue classification methods—i.e., each voxel is assigned to a tissue class mostly according to its signal intensity. In order to make such assignment, the intensity distribution of each tissue class needs to be characterised. This is particularly difficult for some deep GM structures, as differences in signal intensity are very subtle.

Well-known segmentation methods use signal intensity/contrast and prior template-based spatial (i.e., anatomic) information to provide results. The most frequently used semi-automatic brain segmentation algorithms available in free software packages enable 3D image registration and some also use electronic brain atlases to perform voxel classification. Several digital atlases have been developed or improved in order to help segmenting the deep GM.

Other methods have been proposed to segment subcortical structures. Deformable models (curves or surfaces defined within an image domain) have been tried to segment the thalamus. Alternatives to improve segmentation results of deep GM structures also include the use of fuzzy templates or active surface models. Other processing steps to additionally

improve segmentation results encompass template-based statistical properties of shape and appearance supported on probability information estimated by using a training set.

Suggestions for further reading

Amini L., H. Soltanian-Zadeh, *et al.* (2004) "Automatic segmentation of thalamus from brain MRI integrating fuzzy clustering and dynamic contours." *IEEE Transactions on Biomedical Engineering* 51(5): 800–811.
DOI: 10.1109/TBME.2004.826654

Babaloba. K.O., B. Patenaude *et al.* (2009) "An evaluation of four automatic methods of segmenting the subcortical structures in the brain." *NeuroImage* 47(4): 1435–1447.
DOI: 10.1016/j.neuroimage.2009.05.029

Deichmann, R., C.D. Good, *et al.* (2002) "RF inhomogeneity compensation in structural brain imaging." *Magnetic Resonance in Medicine* 47(2): 398–402
DOI: 10.1002/mrm.10050

Fushimi, Y., Y. Miki, *et al.* (2007) "Gray matter-white matter contrast on spin-echo T1-weighted images at 3 T and 1.5 T: a quantitative comparison study." *European Radiology* 17(11): 2921–2925
DOI: 10.1007/s00330-007-0688-9

Liu, Y., B. Li, *et al.* (2006) "Automatic segmentation of putamen from brain MRI." *Lecture Notes in Computer Science* 3973: 606–613
DOI: 10.1007/11760191_89

Liu, J., D. Chelberg, *et al.* (2007) "Automatic subcortical structure segmentation using probabilistic atlas." *Lecture Notes in Computer Science* 4841: 170–178
DOI: 10.1007/978-3-540-76858-6_17

Mazziotta, J.C., A.W. Toga, *et al.* (1995) "A probabilistic atlas of the human brain: theory and rationale for its development. The International Consortium for Brain Mapping (ICBM)." *NeuroImage* 2(2): 89–101
DOI: 10.1006/nimg.1995.1012

Mazziotta, J.C., A.W. Toga, *et al.* (2001) "A probabilistic atlas and reference system for the human brain: International Consortium for Brain Mapping (ICBM)." *Philosophical Transactions of the Royal Society of London. Series B, Biological Sciences* 356(1412): 1293–1322
DOI: 10.1098/rstb.2001.0915

Nitz, W.R., P. Reimer (1999) "Contrast mechanisms in MR imaging." *European Radiology* 9(6): 1032–1046
DOI: 10.1007/s003300050789

Soher, B.J., B.M. Dale, *et al.* (2007) "A Review of MR physics: 3T versus 1.5T." *Magnetic Resonance Imaging Clinics of North America* 15(3): 277–290
DOI: 10.1016/j.mric.2007.06.002

Sreenivas, M., M. Lowry, *et al.* (2007) "A simple solution for reducing artefacts due to conductive and dielectric effects in clinical magnetic resonance imaging at 3 T." *European Journal of Radiology* 62(1): 143–146
DOI: 10.1016/j.ejrad.2006.11.014

Tanenbaum, L.N. (2006) "Clinical 3T MR imaging: mastering the challenges." *Magnetic Resonance Imaging Clinics of North America* 14(1): 1–15
DOI: 10.1016/j.mric.2005.12.004

Tofts, P. (2003) "Quantitative MRI of the brain: measuring changes caused by disease." Editors: Paul Tofts; John Wiley & Sons Ltd. ISBN: 978-0-470-84721-3
DOI: 10.1002/0470869526

Weishaupt, D., V.D. Köchli, *et al.* (2006) "How does MRI work? An introduction to the physics and function of magnetic resonance imaging." Springer, ISBN: 978-3-540-37845-7
DOI: 10.1007/978-3-540-37845-7

Wright, P.J., O.E. Mougin, *et al.* (2008) "Water proton T1 measurements in brain tissue at 7, 3, and 1.5T using IR-EPI, IR-TSE, and MPRAGE: results and optimization." *Magnetic Resonance Materials in Physics, Biology and Medicine* 21(1-2): 121–130
DOI: 10.1007/s10334-008-0104-8

Wu, M., O. Carmichael, *et al.* (2006) "Quantitative comparison of AIR, SPM, and the fully deformable model for atlas-based segmentation of functional and structural MR images." *Human Brain Mapping* 27(9): 747–754
DOI: 10.1002/hbm.20216

Wu, M., C. Rosano, *et al.* (2007) "Optimum template selection for atlas-based segmentation." *NeuroImage* 34(4): 1612–1618
DOI: 10.1016/j.neuroimage.2006.07.050

Zhilkin, P., M.E. Alexander (2004) "Affine registration: a comparison of several programs." *Magnetic Resonance Imaging* 22(1): 55–66
DOI: 10.1016/j.mri.2003.05.004

Zwanenburg, J.J., J. Hendrikse, *et al.* (2010) "Fluid attenuated inversion recovery (FLAIR) MRI at 7 Tesla: comparison with 1.5 and 3.0 Tesla." *European Radiology* 20(4): 915–922
DOI: 10.1007/s00330-009-1620-2

Attached publication

Clinical Radiology 71 (2016) 1304–1308

Contents lists available at ScienceDirect

Clinical Radiology

journal homepage: www.clinicalradiologyonline.net

Technical Report

Magnetisation-prepared rapid gradient-echo versus inversion recovery turbo spin-echo T1-weighted images for segmentation of deep grey matter structures at 3 T

S. Brandão [a], A.J. Bastos-Leite [b,*]

[a] Department of Radiology, Hospital de São João, Porto, Portugal
[b] Department of Medical Imaging, University of Porto, Faculty of Medicine, Porto, Portugal

ARTICLE INFORMATION

Article history:
Received 14 August 2015
Received in revised form
19 August 2016
Accepted 8 September 2016

Introduction

The single-slab three-dimensional (3D) magnetisation-prepared rapid gradient-echo (MPRAGE) magnetic resonance imaging (MRI) sequence is often used to acquire T1-weighted images (T1-WI) of the brain allowing multiplanar reconstruction and displaying high contrast between grey (GM) and white matter (WM).[1] 3D MPRAGE T1-WI are also frequently used for volumetric analyses of the brain involving segmentation of the GM; however, previous MRI studies have shown that inversion recovery (IR) turbo spin-echo (TSE) T1-WI display higher contrast and can be more accurate than other types of T1-WI for the differentiation between subcortical GM and WM.[2]

MRI systems operating at 3 T have been generally introduced in clinical practice during the past decade.[3] 3 T MRI usually allows the acquisition of better quality images than lower field-strength systems, but the increase in T1 relaxation times[4] and the occurrence of "standing wave" effects at high field-strength[5] may lead to a lack of contrast between deep GM structures and the surrounding WM on T1-WI.

The purpose of the present study was to compare 3D MPRAGE with IR TSE T1-WI acquired at 3 T as input images to segment the striatum and thalamus.

Materials and methods

All procedures involving human participants included in this study were in accordance with the ethical standards of the institutional research committee and with the 1964 Helsinki declaration or its later amendments.

Participants

The sample for this study comprised 30 healthy volunteers (15 women, mean age=32 years, standard deviation [SD]=5.1).

MRI protocol

MRI data were acquired using a scanner operating at 3 T (Magnetom Trio, A Tim System, Siemens, Erlangen, Germany) and equipped with a 12-channel radiofrequency (RF) head coil. To obtain whole-brain coverage, sagittal single-slab 3D MPRAGE T1-WI were acquired (echo time [TE]=3 ms, repetition time [TR]=2,300 ms, flip angle=9°,

* Guarantor and correspondent: A.J. de Bastos Leite, University of Porto, Faculty of Medicine, Department of Medical Imaging, Alameda do Professor Hernâni Monteiro, 4200–319 Porto, Portugal. Tel.: +351 938382287; fax: +351 225500531.
E-mail address: abastosleite@med.up.pt (A.J. Bastos-Leite).

http://dx.doi.org/10.1016/j.crad.2016.09.009

inversion time [TI]=900 ms, field of view [FOV]=240 mm, section thickness=1.2 mm, number of sections=160, acquisition matrix=256×256, voxel resolution=1×1×1.2 mm, scanning time=9:14 minutes). Axial IR TSE T1-WI were also acquired (TE=15 ms, TR=4,300 ms, flip angle=60°, TI=400 ms, FOV=240 mm, section thickness=3 mm, no inter-section gap, number of sections=44, acquisition matrix=256×256, voxel resolution=0.9×0.9×3 mm, scanning time=6:16 minutes). The choice of parameters (e.g., TI) was based on previous studies addressing the optimisation of similar MRI sequences.[6,7] Parameters used to acquire 3D MPRAGE T1-WI were the specifically recommended for the MRI system used, according to the Alzheimer's Disease Neuroimaging Initiative (ADNI) multicentre study.[8]

Image analysis

Signal-to-noise ratios (SNR) of deep GM structures on 3D MPRAGE and IR TSE T1-WI were calculated, dividing the signal intensity in regions of interest (ranging from 18.3 to 26.1 mm^2) localised at the head of the caudate nucleus, anterior part of the putamen, posterior part of the putamen, and in the thalamus—on each side of the midline—by the standard deviation (SD) of noise. Contrast-to-noise ratios (CNR) of the deep GM relative to the WM were also calculated, dividing the corresponding difference in signal intensity by the SD of noise. Regions of interest to measure the signal intensity of the deep WM (ranging from 10.2 to 15.3 mm^2) were localised in the genu of each internal capsule. The SD of noise was obtained from a background region of air with approximately 120 mm^2. SNR and CNR calculated on pre-processed images from a subset of 15 randomly selected participants were compared between sequences.

A standard segmentation algorithm[9] available from the Statistical Parametric Mapping (SPM) software (http://www.fil.ion.ucl.ac.uk/spm/) was applied on 3D MPRAGE and IR TSE T1-WI of the entire sample. The default segmentation routine implemented in SPM5 was used, which performs tissue segmentation, registration, and intensity non-uniformity (bias) correction in a unified model. The principal idea of this method is to model image intensities as a mixture of Gaussians, in which the mean, variance, and a mixing proportion model each Gaussian cluster. Modified versions of tissue probabilistic atlases from the International Consortium for Brain Mapping are used to provide prior information about the tissue classes, and the Bayes rule is used to create the posterior probability of each class. Therefore, this segmentation routine assigns a probability value to each voxel as belonging to a given class based upon the corresponding signal intensity and contrast on the input images. Moreover, this algorithm is commonly used for automatic volumetric analyses of the brain (e.g., voxel-based morphometry).[10]

The GM probability maps obtained from images of each sequence were co-registered, spatially normalised to the standard Montreal Neurological Institute template at a spatial resolution of 1×1×1 mm, and converted to binary masks at a threshold of 0.2. This is a common masking threshold suggested for voxel-based morphometry.[11] Deep GM voxels corresponding to the striatum and thalamus on binary masks were then separated from the rest of cerebral GM by manually excluding cortical GM voxels. The mean volumes of the striatum and thalamus on binary masks were calculated and compared between sequences. A deep GM mask, created after binarising probability maps of the Harvard–Oxford subcortical structural atlas, at a threshold of 0.2, was used as the reference standard for quantification.

Taking the mask created after binarising probability maps of the Harvard–Oxford subcortical structural atlas as the reference standard for visual inspection as well, differences in voxel classification between binary masks obtained after segmentation of GM on 3D MPRAGE and IR TSE T1-WI were assessed in consensus by two observers (S.B. and A.J.B.-L.) in the following four regions: anterior part of the striatum, posterior part of the striatum, medial part of the thalamus, and lateral part of the thalamus. The cross point of the boundaries for these regions on each side of the midline was considered to be the genu of the internal capsule (Fig 1).

Statistical analysis

Statistical analysis was carried out using IBM SPSS 22.0 (www.ibm.com/software/analytics/spss/). Given that the SNR of deep GM structures, the CNR of the deep GM relative to the WM, and the volumes of the deep GM had an approximately normal distribution, the paired-samples Student's *t*-test was used to compare their means. Statistical significance was considered when $p<0.05$.

Results

Table 1 presents the SNR of the deep GM structures and the CNR of the deep GM relative to the WM. The CNR of the deep GM relative to the WM were found to be significantly higher on IR TSE T1-WI ($p<0.001$). The lowest CNR of the deep GM relative to WM were found on 3D MPRAGE T1-WI in the posterior part of the putamen and in the thalamus.

The mean volume of the striatum and thalamus calculated after segmentation of the GM on 3D MPRAGE T1-WI was 24.1 cm^3 (SD=3.25), whereas the corresponding volume using IR TSE T1-WI was 26.3 cm^3 (SD=4.01). The difference in volumes between sequences was found to be statistically significant ($p<0.001$). Taking the mask created after binarising probability maps of the Harvard–Oxford subcortical structural atlas as the reference standard for quantification, binary masks obtained after segmentation of the GM were found to represent up to 76% of the reference volume (mean=47%; minimum=39%) using IR TSE T1-WI, and up to 65% of the reference volume (mean=43%; minimum=34%) using 3D MPRAGE T1-WI.

Based on visual inspection taking the mask created after binarising probability maps of the Harvard–Oxford subcortical structural atlas as the reference standard, differences in voxel classification between binary masks obtained after segmentation of the GM on 3D MPRAGE T1-WI and those obtained after segmentation of the GM on IR TSE

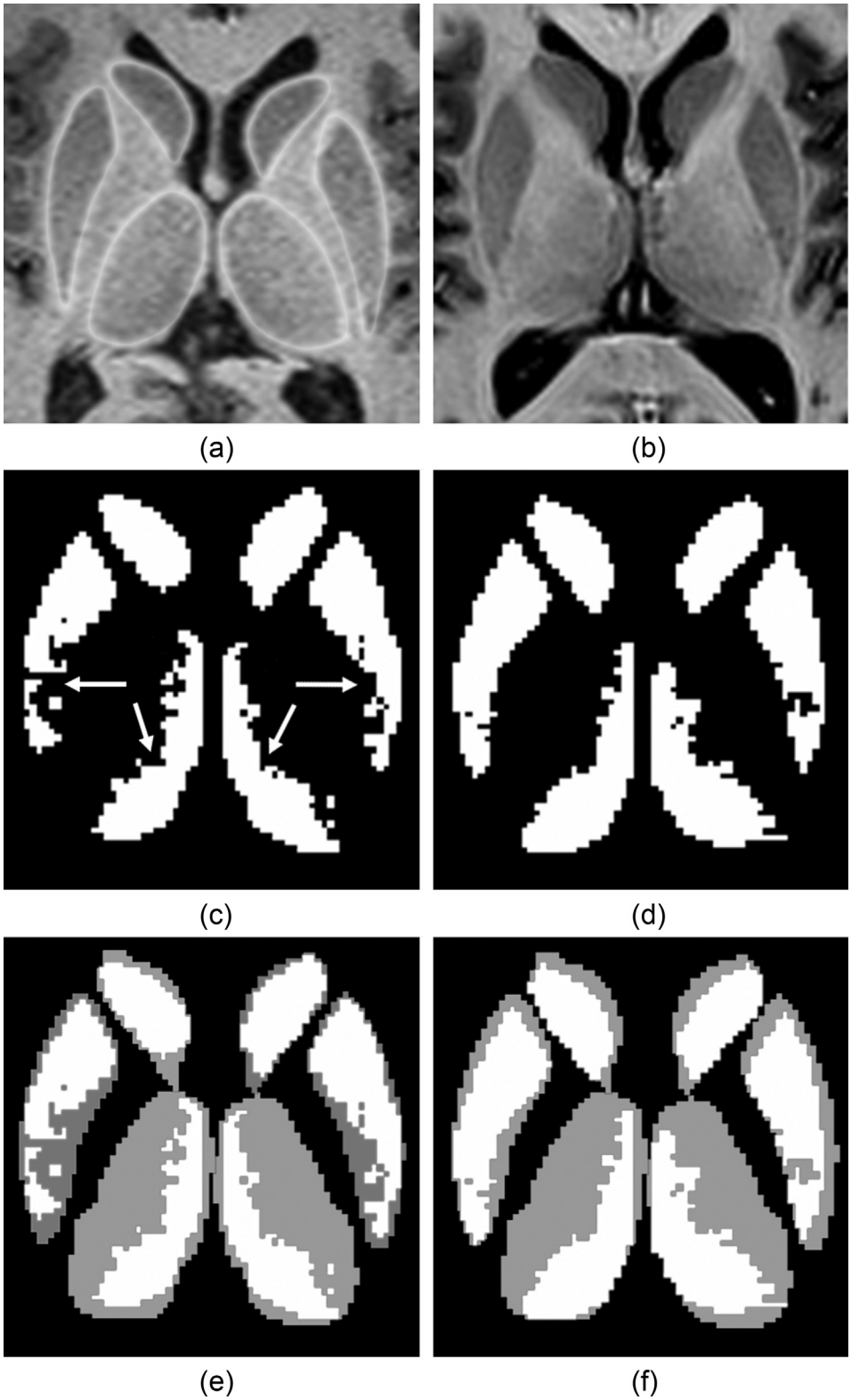

Figure 1 (a–b) Pre-processed T1-WI from one participant showing the caudate nuclei, putamina, and thalami. (a) The limits (white line) of these structures were drawn on a 3D MPRAGE T1-weighted image reformatted into the axial plane for visualisation purposes. (b) Note the higher contrast of deep GM relative to WM on the IR TSE T1-weighted image. (c–d) Binary masks obtained after segmentation of the GM on 3D MPRAGE (c) and IR TSE (d) T1-WI. Note the fewer number of deep GM voxels (in white) on the binary mask obtained after segmentation of the GM on 3D MPRAGE T1-WI (c), especially in the posterior part of the putamina (horizontal arrows) and in the thalami (oblique arrows). (e–f) Binary masks obtained after segmentation of the GM on 3D MPRAGE and IR TSE T1-WI superimposed on a mask created after binarising probability maps of the caudate nuclei, putamina, and thalami from the Harvard–Oxford subcortical structural atlas (in grey).

Table 1
Signal-to-noise ratios (SNR) of the deep grey matter, and contrast-to-noise ratios (CNR) of the deep grey matter relative to white matter in the regions of interest (ROI) on three-dimensional (3D) magnetisation prepared rapid gradient-echo (MPRAGE) and inversion recovery (IR) turbo spin-echo (TSE) T1-weighted images (T1-WI).

ROI	Mean SNR (standard deviation)[a]		*p*-Value	Mean CNR (standard deviation)[a]		*p*-Value
	3D MPRAGE T1-WI	IR TSE T1-WI		3D MPRAGE T1-WI	IR TSE T1-WI	
Head of right caudate	56.9 (5.32)	75.6 (19.68)	<0.01	29.5 (3.15)	68.8 (18.58)	<0.001
Head of left caudate	58.9 (5.62)	77.2 (19.40)	<0.01	29.0 (2.91)	73.8 (18.52)	<0.001
Anterior part of the right putamen	58.8 (6.16)	65.1 (17.94)	0.21	27.6 (2.74)	58.3 (16.26)	<0.001
Anterior part of the left putamen	63.6 (6.38)	71.2 (19.10)	0.15	24.3 (2.88)	64.5 (18.23)	<0.001
Posterior part of the right putamen	69.0 (6.47)	49.1 (13.54)	<0.001	17.4 (2.61)	42.3 (12.53)	<0.001
Posterior part of the left putamen	71.6 (6.40)	50.2 (13.01)	<0.001	16.4 (2.52)	43.4 (12.01)	<0.001
Right thalamus	78.1 (7.28)	29.9 (8.40)	<0.001	8.4 (3.63)	23.1 (8.70)	<0.001
Left thalamus	79.9 (8.30)	30.5 (9.17)	<0.001	8.1 (3.07)	23.7 (9.10)	<0.001
Average	67.1 (6.35)	56.1 (14.80)	<0.05	20.1 (2.41)	49.7 (13.72)	<0.001

[a] Values calculated on pre-processed 3D MPRAGE and IR TSE T1-WI.

T1-WI were found to occur especially in the posterior part of the striatum and in the lateral part of the thalamus. Although none of the structures could be entirely segmented in any participant, IR TSE T1-WI were found to be better than 3D MPRAGE T1-WI to represent the posterior part of the striatum and the lateral part of the thalamus (Fig 1) in all participants.

Discussion

The results of the present study showed that IR TSE T1-WI enable better segmentation of the striatum and thalamus than 3D MPRAGE T1-WI. This is in agreement with previous data indicating that IR T1-weighted sequences provide images with higher contrast than other types of T1-WI to represent subcortical structures.[2]

3D MPRAGE and related sequences, such as the spoiled gradient recalled (SPGR) echo sequence, are considered to be the sequences of choice when detailed anatomical or multiplanar reconstruction is required, and most of the currently existing methodological approaches concerning automatic volumetric analyses of the brain rely on their use to generate input images.[10,12] There is also no current alternative that can generally replace these sequences in clinical practice; however, a potential drawback of the corresponding images can be considered, especially when interpreting the results of automatic volumetric studies using 3D MPRAGE T1-WI, as the present findings indicate that a significant part of the striatum and thalamus cannot be taken into account after a standard segmentation of the GM.

Crucially, the lowest CNR of the deep GM relative to the WM were found on 3D MPRAGE T1-WI in the posterior part of the putamen and in the thalamus (Table 1). The significantly higher CNR of deep GM relative to WM on IR TSE T1-WI justify why these images warrant a better representation of the posterior part of the striatum and the lateral part of the thalamus than the one provided by 3D MPRAGE T1-WI. Nevertheless, none of the structures could be entirely segmented in any participant.

The lack of contrast of the posterior part of the putamen on T1-WI may be secondary to its high iron content, which is probably an overlooked factor contributing to contrast on T1-WI. As a matter of fact, although the iron content is mostly believed to have an effect on T2 relaxation times, its presence in the brain also influences T1 relaxation times,[13] and hence the GM to WM contrast on T1-WI. Likewise, the high signal intensity of the thalamus on T1-WI attributable to its higher myelin content—compared to the cortical GM and the basal ganglia—diminishes the contrast between its lateral part and the adjacent posterior limb of the internal capsule (Fig 1).

An alternative explanation for the differences observed in the present study could be based upon characteristics of the analysed images other than contrast, such as the SNR. Nonetheless, the SNR was found to be significantly lower on IR TSE T1-WI in the posterior part of the putamen and in the thalamus (Table 1).

Alternatively, other segmentation algorithms could have provided different results, and the optimum threshold to create binary masks from GM probability maps might vary and be dependent on the chosen MRI sequence. It is, therefore, conceivable that the observed results in the current study could have been dependent both on the applied segmentation method and on the threshold used to create binary masks. Nevertheless, the rationale to use just one standard segmentation approach for both sequences, and the same threshold to create binary masks, certainly had the advantage of avoiding confounders that would arise from comparing different segmentation algorithms, or different thresholds, for different MRI sequences.

Furthermore, to circumvent the absence of a true gold standard towards what could be determined the most accurate volume of the deep GM after segmentation in individual participants, and to ascertain which of the imaging sequences afforded better representation of the striatum and thalamus, a deep GM mask created after binarising probability maps of the Harvard–Oxford subcortical structural atlas was used, at the same threshold (i.e., 0.2), as an effective reference (Fig 1).

A limitation of the current study was the relatively small sample size and a limited age span restricted to young individuals. The inclusion of older participants could possibly represent an advantage, namely to clarify the influence of

iron deposition in the brain, which typically increases with ageing. Another limitation of the present study can be attributable to the fact that a single-slab 3D MRI sequence was compared with a two-dimensional one. Therefore, given that images from each sequence were acquired with different section thickness and different in-plane resolution, an error in the process of their normalisation might have occurred due to partial volume effects secondary to the larger voxel volumes on pre-processed IR TSE T1-WI (2.43 mm^3 versus 1.2 mm^3 on 3D MPRAGE T1-WI). It is, however, very unlikely that such an error could have accounted for the reported differences, which were mainly noticeable in the lateral part of the thalamus and in the posterior part of the striatum (Fig 1) across participants. In other words, there is no explanation for a predilection of partial volume effects for these particular regions.

Other T1-weighted MRI sequences, still not currently implemented in clinical practice, may serve as better alternatives to visualise the brain in the future. Phase-sensitive T1 IR[14] and fast GM acquisition T1 IR[15] represent examples of novel MRI sequences that improve the visualisation of deep GM structures.

MRI sequences exploring sources of contrast other than T1 relaxation alone, such as magnetisation transfer maps obtained from fast low-angle shot or spoiled gradient-echo sequences have been shown to represent another possibility to enhance tissue characterisation,[16,17] and to improve segmentation results for several deep cerebral and infratentorial GM structures.[17] Furthermore, by combining several image contrasts (e.g., T1 and T2), it is also possible to better visualise deep GM nuclei. Multispectral (i.e., multicontrast) segmentation routines seem to be very promising indeed to provide even more reliable brain tissue characterisation in the future.

In conclusion, IR TSE serves as a better source of T1-WI than 3D MPRAGE to segment the posterior part of the striatum and the lateral part of the thalamus.

Acknowledgements

The authors are indebted to Sérgio Ferreira for assistance with the layout of the illustration.

References

1. Brant-Zawadzki M, Gillan GD, Nitz WR. MP RAGE: a three-dimensional, T1-weighted, gradient-echo sequence—initial experience in the brain. *Radiology* 1992;**182**(3):769–75.
2. Reich CA, Hudgins PA, Sheppard SK, *et al*. A high-resolution fast spin-echo inversion-recovery sequence for preoperative localization of the internal globus pallidus. *AJNR Am J Neuroradiol* 2000;**21**(5):928–31.
3. Frayne R, Goodyear BG, Dickhoff P, *et al*. Magnetic resonance imaging at 3.0 Tesla: challenges and advantages in clinical neurological imaging. *Invest Radiol* 2003;**38**(7):385–402.
4. Stanisz GJ, Odrobina EE, Pun J, *et al*. T1, T2 relaxation and magnetization transfer in tissue at 3 T. *Magn Reson Med* 2005;**54**(3):507–12.
5. Tropp J. Image brightening in samples of high dielectric constant. *J Magn Reson* 2004;**167**(1):12–24.
6. Nakamura H, Yamada K, Kizu O, *et al*. Optimization of TI values in inversion-recovery MR sequences for the depiction of fine structures within gray and white matter: separation of globus pallidus interna and externa. *Acad Radiol* 2003;**10**(1):58–63.
7. Lin C, Bernstein MA. 3D magnetization prepared elliptical centric fast gradient echo imaging. *Magn Reson Med* 2008;**59**(2):434–9.
8. Mueller SG, Weiner MW, Thal LJ, *et al*. The Alzheimer's disease neuroimaging initiative. *Neuroimaging Clin N Am* 2005;**15**(4):869–77. xi–xii.
9. Ashburner J, Friston KJ. Unified segmentation. *Neuroimage* 2005;**26**(3):839–51.
10. Ashburner J, Friston KJ. Voxel-based morphometry—the methods. *Neuroimage* 2000;**11**(6 Pt 1):805–21.
11. Ashburner J. *VBM Tutorial*. 2010. Available at: http://www.fil.ion.ucl.ac.uk/~john/misc/VBMclass10.pdf [27 April 2015].
12. Cardoso MJ, Clarkson MJ, Ridgway GR, *et al*. LoAd: a locally adaptive cortical segmentation algorithm. *Neuroimage* 2011;**56**(3):1386–97.
13. Ogg RJ, Steen RG. Age-related changes in brain T1 are correlated with iron concentration. *Magn Reson Med* 1998;**40**(5):749–53.
14. Hou P, Hasan KM, Sitton CW, *et al*. Phase-sensitive T1 inversion recovery imaging: a time-efficient interleaved technique for improved tissue contrast in neuroimaging. *AJNR Am J Neuroradiol* 2005;**26**(6):1432–8.
15. Sudhyadhom A, Haq IU, Foote KD, *et al*. A high resolution and high contrast MRI for differentiation of subcortical structures for DBS targeting: the Fast Gray Matter Acquisition T1 Inversion Recovery (FGATIR). *Neuroimage* 2009;**47**(Suppl. 2):T44–52.
16. Gringel T, Schulz-Schaeffer W, Elolf E, *et al*. Optimized high-resolution mapping of magnetization transfer (MT) at 3 Tesla for direct visualization of substructures of the human thalamus in clinically feasible measurement time. *J Magn Reson Imaging* 2009;**29**(6):1285–92.
17. Helms G, Draganski B, Frackowiak R, *et al*. Improved segmentation of deep brain grey matter structures using magnetization transfer (MT) parameter maps. *Neuroimage* 2009;**47**(1):194–8.